Flexible distillation test rig on a laboratory scale for characterization of additively manufactured packings

Johannes Neukäufer[1]*, Nadin Sarajlic[2], Harald Klein[2], Sebastian Rehfeldt[2], Heiko Hallmann[3], Carsten Knösche[3], Thomas Grützner[1]

[1] Ulm University, Institute of Chemical Engineering, Laboratory of Thermal Process Engineering, Albert-Einstein-Allee 47, 89081 Ulm, Germany

[2] Technical University of Munich, Department of Mechanical Engineering, Institute of Plant and Process Technology, 85748 Garching, Germany

[3] BASF SE, 67056 Ludwigshafen am Rhein, Germany

Correspondence: M.Sc. Johannes Neukäufer (johannes.neukaeufer@uni-ulm.de), Ulm University, Institute of Chemical Engineering, Laboratory of Thermal Process Engineering, Albert-Einstein-Allee 47, 89081 Ulm, Germany

Abstract

Additive manufacturing is increasingly being used to develop innovative packings for absorption and desorption columns. Since distillation has not been in focus so far, this paper aims to fill this gap. The objective is to obtain a miniaturized 3D printed packed column with optimized properties in terms of scalability and reproducibility, which increases process development efficiency. For this purpose, a flexible laboratory scale test rig is presented combining standard laboratory equipment with 3D printed components such as innovative multifunctional trays or the column wall with packing. The test rig offers a particularly wide operating range $\left(F = 0.15\,\mathrm{Pa}^{0.5} \ldots\ 1.0\,\mathrm{Pa}^{0.5}\right)$ for column diameters between $20\,\mathrm{mm}$ and $50\,\mathrm{mm}$. First results regarding the time to reach steady-state, operational stability and separation efficiency measure-

ments are presented using a 3D printable version of the Rombopak 9M. Currently, further developed and newly designed packing structures are being characterized, which should exhibit optimized properties especially with respect to scalability and separation efficiency.

Topical heading

Separations: Materials, Devices and Processes

Keywords

Additive manufacturing, packed column, distillation, mass transfer, 3D printing

1 Introduction

Distillation, as the most important thermal separation process, is usually carried out in packed or tray columns [1]. Packed columns have a higher capacity than tray columns of the same diameter, since the downcomer in tray columns, which is not contributing to separation, usually occupies a part of the column cross sectional area [2]. Another advantage of packed columns is the significantly lower pressure drop. In the chemical industry, this results in an increasing trend towards the construction of packed columns. However, these are characterized by greater uncertainties with respect to design, especially due to maldistribution [1]. For well-established distillation separation tasks, the risk for a failed large-scale industrial implementation has already been minimized to a large extent. Major problems arise in the development of novel distillation tasks with new chemicals. The number of new chemicals commercially produced per year ranges from 500 to 2000 [3–5]. Most of these chemicals have to be purified in distillation columns after synthesis. As a result, an increasing need for optimization in process development can be derived for the separation of components by means of distillation.

Preliminary investigations in suitable laboratory scale test columns are often indispensable before large scale implementation. The small diameters used in this process lead to great uncertainties when transferring the obtained results to industrial scale columns. As a consequence, high safety margins are used, which correlate with larger column heights. Conventional column or packing manufacturing methods have not yet been able to find an adequate solution to this problem.

However, miniaturized packed columns bring a variety of advantages. Small column diameters are associated with a reduced amount of chemicals needed for experiments. Usually, these are produced in the laboratory by multi-step synthesis resulting in high costs and an increasing time investment. Furthermore, the test rig acquisition costs could be reduced, since these scale

with the throughput of the column. In addition, lower safety requirements and less space in the usually expensive fume hood areas are needed.

Nevertheless, the problem of miniaturized packed columns for distillation presents a number of challenges. For small-diameter columns, effects such as increased liquid wall flow and lack of adiabasia are exacerbated by an increased column wall-to-packing ratio [6]. As a lower scalability limit, values between $40\,\mathrm{mm}$ and $100\,\mathrm{mm}$ are given for the column diameter from various sources [7]. Conventional manufacturing processes are reaching their limits when it comes to miniaturizing the columns. As a solution, additive manufacturing could provide a remedy due to the high degree of freedom in design [8].

3D printing is widely used in chemical reaction engineering and catalysis [9–11]. Here, zeolites or periodic open-cellular structures are often used as supports for catalysts. Gradually, more and more publications are appearing in which novel 3D printed packing structures are used and/or characterized for thermal separation technology [12–14]. While the majority of publications focus on the areas of rotating packed beds [15–17] or absorption and desorption [18–22], there are hardly any publications specifically for distillation [23].

This publication aims to fill this gap by presenting a laboratory scale distillation test rig specifically designed for characterization of small scale packings with the focus on additively manufactured structures. The test facility is characterized by a particularly wide operating range and a high degree of flexibility, so that even miniaturized columns can be adequately investigated. Gas loads between $F = 0.15\,\mathrm{Pa}^{0.5}$ and $F = 1.0\,\mathrm{Pa}^{0.5}$ can be realized for column diameters between $D = 20\,\mathrm{mm}$ and $D = 50\,\mathrm{mm}$. Not only the packings, but the entire column apart from the standard laboratory equipment is manufactured additively. 3D printed multifunctional trays above and below the column are used for sampling, liquid inlet/outlet or insertion of temperature and differential pressure drop sensors. The different design approaches as well as

the results of packing structures already tested in the plant will be presented. The original design approaches are based on the methodology of a previous publication [24]. However, this contribution will focus on the experimental design and operation of the test rig.

2 Separation efficiency at total reflux

The characterization of packings is usually performed in distillation columns operated at total reflux using appropriate binary reference systems [25]. Common reference systems are, for example, ethylbenzene/chlorobenzene, *o*-xylene/*p*-xylene or *n*-heptane/cyclohexane (nHep/cHex), which have a particularly advantageous ideal behavior and largely constant relative volatilities [26]. The content here should deal with the system nHep/cHex as an example. In most cases, the separation efficiency of a packing is indicated by the height equivalent to a theoretical plate (*HETP*) or its reciprocal, the number of theoretical stages per meter packed height (*NTSM*). The standard representation of the separation efficiency is given by the plot of the *HEPT* value over the gas load (*F*-factor).

Accordingly, the *HETP* value is dependent on the *F*-factor in the column. The *F*-factor is defined in Equation (2.1), where u_G represents the superficial gas velocity and ρ_G the gas density.

$$F = u_G \cdot \rho_G^{0.5} \tag{2.1}$$

Knowing the gas mass flow rate $\dot{m}_G$, usually measured at the top of the column, and the column cross-sectional area A_C, or rather the column diameter d_C, the gas velocity u_G can be calculated according to Equation (2.2).

$$u_G = \frac{\dot{m}_G}{\rho_G \cdot A_C} = \frac{\dot{m}_G}{\rho_G \cdot \frac{\pi}{4} \cdot D_C^2} \tag{2.2}$$

The gas density ρ_G can be calculated to a good approximation for the common reference systems at atmospheric conditions using the ideal gas law (see Equation (2.3)). Here, p represents the pressure and M_G the molar mass of the respective gas phase, w the mass fraction and M_{cHex} and M_{nHep} the molar mass of the pure components cHex and nHep.

$$\rho_{\mathrm{G}} = \frac{p \cdot M_{\mathrm{G}}}{R \cdot T} \quad \text{with} \quad \frac{1}{M_{\mathrm{G}}} = \frac{1}{\frac{w_{\mathrm{cHex}}}{M_{\mathrm{cHex}}} + \frac{w_{\mathrm{nHep}}}{M_{\mathrm{nHep}}}} \tag{2.3}$$

After calculating the liquid densities ρ_{L} from the pure densities as shown in the Attachment A (see Equation (A.1) and (A.4)) at the top of the column, the liquid load B can be calculated according to Equation (2.4).

$$B = u_{\mathrm{G}} \cdot \frac{\rho_{\mathrm{G}}}{\rho_{\mathrm{L}}} = F \cdot \frac{\rho_{\mathrm{G}}^{0.5}}{\rho_{\mathrm{L}}} \tag{2.4}$$

It can be deduced from Equation (2.3) that the gas density along the column is not constant, since the molar mass of the mixture, the temperature and the pressure vary over the column height. The symbols marked with a superscript T describe the condition at the top and the symbols marked with a superscript B describe the condition at the bottom of the column. Accordingly, the gas densities must be determined for the top and the bottom of the column, as shown in Equation (2.5). Here, the universal gas constant is represented by R and the temperature by T. Since the pressure p is usually set at the top of the column, the pressure drop Δp of the packing also appears in the calculation of the gas density at the bottom and must be taken into account accordingly.

$$\rho_{\mathrm{G}}^{\mathrm{T}} = \frac{p \cdot M_{\mathrm{G}}^{\mathrm{T}}}{R \cdot T^{\mathrm{T}}} \quad \text{and} \quad \rho_{\mathrm{G}}^{\mathrm{B}} = \frac{\left(p + \Delta p\right) \cdot M_{\mathrm{G}}^{\mathrm{B}}}{R \cdot T^{\mathrm{B}}} \tag{2.5}$$

The different gas densities result in different F-factors at the top and the bottom of the column. The assumption of constant enthalpies of evaporation of both components leads to constant molar flows along the column when operating under total reflux. However, there is another effect that must be taken into account. For analysis purposes and for measuring the mass flow at the top of the column, the distillate stream is often led out of the column and returned to the top of the column again. In this process, the liquid is usually subcooled to a certain extend. The subcooled liquid leads to additional condensation of the rising vapor in the column, which

influences the liquid and gas flow accordingly. The latent heat of condensation brings the previously subcooled liquid to boiling temperature. At the top of the column, the leaving gas mass flow rate and the liquid mass flow rate reentering the column are equal. The latter can be determined in the distillate circuit. The gas mass flow at the bottom of the column, on the other hand, can be calculated by Equation (2.6), taking into account the degree of distillate subcooling [27]. Variables with a superscript R refer to the state of the distillate reflux flow stream. In Equation (2.6), the mass flow at the bottom is corrected by considering the enthalpy difference of the top and of the reflux relative to the enthalpy of evaporation Δh_V at the bottom. While the temperatures T^T at the top and T^R of the reflux are usually measured, the according specific heat capacities $c_{p,L}^T$ and $c_{p,L}^R$ can be calculated on the basis of pure component correlation equations as explained in Attachment A.

$$\dot{m}_G^B = \dot{m}_G^T \cdot \left[1 + \frac{c_{p,L}^T \cdot T^T - c_{p,L}^R \cdot T^R}{\Delta h_V^B} \right] \tag{2.6}$$

By combining Equations (2.1) and (2.2) and averaging over the top and bottom of the column, a representative average *F*-factor is obtained as shown in Equation (2.7).

$$F_{avg} = \frac{1}{2} \cdot \left[\frac{\dot{m}_G^T}{\sqrt{\rho_G^T} \cdot \left(\frac{\pi}{4} \cdot d_C^2 \right)} + \frac{\dot{m}_G^B}{\sqrt{\rho_G^B} \cdot \left(\frac{\pi}{4} \cdot d_C^2 \right)} \right] \tag{2.7}$$

For the common test systems, the Fenske equation [28] can be used with good approximation to calculate the theoretical number of stages N_{th} for distillation columns operated with total reflux. This is shown in Equation (2.8), where α_{avg} is the average relative volatility, x_{cHex}^T represents the low-boiling-component molar fraction in the distillate and x_{cHex}^B in the bottom, respectively.

$$N_{th} = \frac{\ln \left[\left(\frac{x_{cHex}^T}{1 - x_{cHex}^T} \right) \cdot \left(\frac{1 - x_{cHex}^B}{x_{cHex}^B} \right) \right]}{\ln \left(\alpha_{avg} \right)} \tag{2.8}$$

Due to the fact that the relative volatility α usually cannot be assumed to be constant over the column height, it has to be averaged over the considered concentration range with *m* supporting points, as shown in Equation (2.9).

$$\alpha_{\text{avg}} = \left(\prod_{i}^{m} \alpha_i \right)^{\frac{1}{m}} \tag{2.9}$$

The corresponding relative volatilities α_i are obtained from the experimental data of the equilibrium curve of the considered system and can be calculated according to Equation (2.10). The index *i* refers to supporting points *i*, by means of which the averaged relative volatility is calculated. $y_{\text{cHex},i}$ and $x_{\text{cHex},i}$ describe the molar fractions of the gas and liquid phases of the light boiling component (cHex) in equilibrium.

$$\alpha_i = \frac{x_{\text{cHex},i} \cdot y_{\text{cHex},i} - y_{\text{cHex},i}}{x_{\text{cHex},i} \cdot y_{\text{cHex},i} - x_{\text{cHex},i}} \tag{2.10}$$

The vapor liquid equilibrium of the system nHep/cHex can be described with the experimental data of Onken et al. [26]. To calculate the average relative volatility α_{avg}, several supporting points *i* can be used in the concentration range considered. If many supporting points are selected, the error can be minimized. Since the height of the packing H_{P} is known, the *HETP* value of the packing can be determined according to Equation (2.11) knowing the theoretical number of stages N_{th} from Equation (2.8).

$$HETP = \frac{H_{\text{P}}}{N_{\text{th}}} \tag{2.11}$$

3 Distillation test rig

The test rig for the characterization of additively manufactured (3D printed) packings is illustrated in Figure 1. While the piping and instrumentation diagram (P&ID) on the left gives a detailed overview of the plant features, the photo of the plant shown on the right provides a more detailed idea of its implementation and the design. The test facility is located inside an aluminum framework on rolls within a conventional walk-in fume hood with an effective

height of 2.45 m. The process control system is easily adaptable by using the software LabVIEW^{TM}. The plant is currently operated with the system cHex/nHep. However, other standard reference systems can also be investigated at a later stage. The plant is operated under atmospheric conditions, but later also under vacuum. The denotation of the test rig components in the following sections always refers to the P&ID diagram in Figure 1.

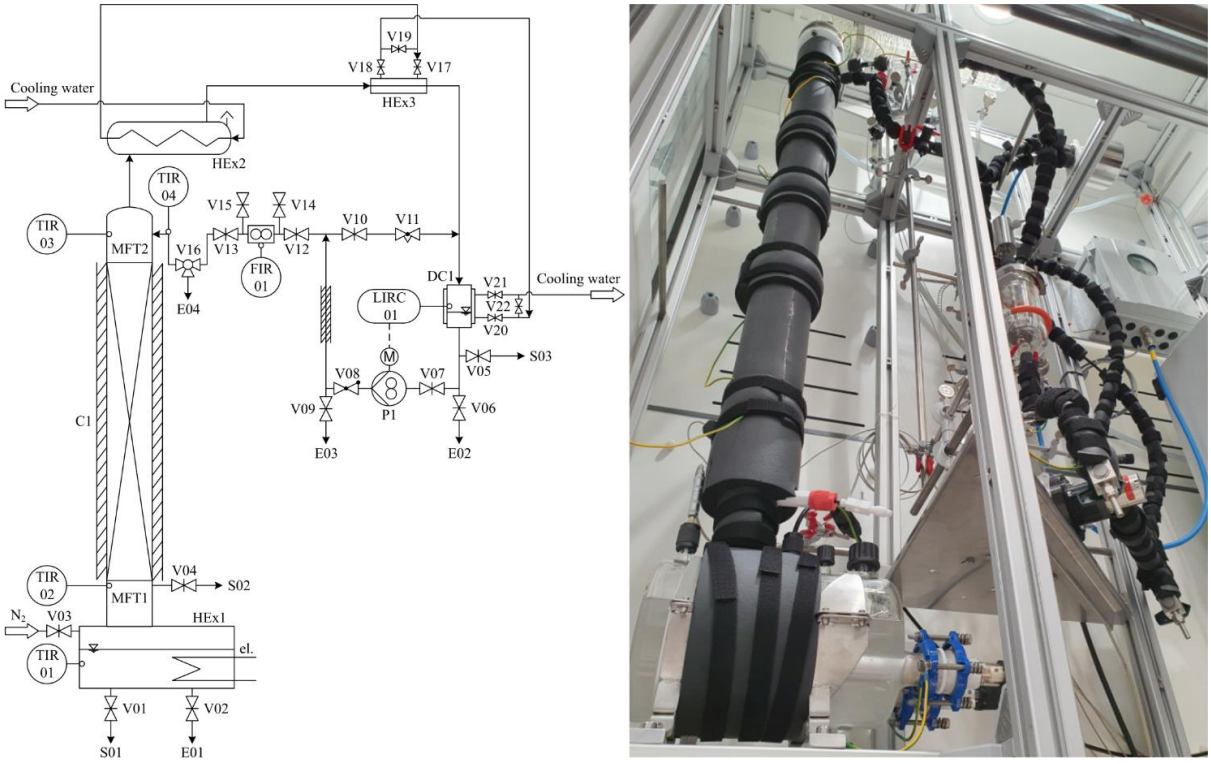

Figure 1: Piping and instrumentation diagram (left) and photograph (right) of the test rig for characterization of additively manufactured packings.

3.1 Reboiler

The reboiler HEx1 is designed as a glass container with two heating rods. The maximum heat duty is 1.8 kW, which is available for the evaporation of about 2.5 l of the system. For safety reasons, it would be advantageous to implement the evaporator by means of heating hoods or by using thermal fluids. However, the necessary heating capacity for flexible operation for columns with diameters between $D = 20\,\mathrm{mm}$ and $D = 50\,\mathrm{mm}$ could only be realized with heating rods due to the limited space. The intention was to be able to provide sufficient vapor corresponding to a F-factor of at least $F = 1.0\,\mathrm{Pa}^{0.5}$ also at the maximum column diameter of

$D = 50\,\mathrm{mm}$. For smaller column diameters correspondingly larger gas loads can be realized. This operating range is typical for small-scale laboratory test columns. The TIR01, designed as a Pt100, can be used to record the temperature in the HEx1 during operation. A sample S01 can be taken via the valve V01. Valve V02 is used to drain the reboiler. Valve V03 is used to inject nitrogen for initial inertization of the system, so that an explosive environment is avoided. Further connections for filling or retrofitting are available.

3.2 Additively manufactured components

The multifunctional tray MFT1 below the packing, MFT2 above the packing and the column C1 with shell and packing shown in Figure 1 were produced using 3D printing. The components were manufactured using the selective laser sintering (SLS) method with polyamide 12 (PA12) as printing material and infiltrated afterwards at the external 3D printing provider Blue Production GmbH & Co. KG. Additive manufacturing from plastic was preferred over metal printing, as the latter is far more expensive. However, polyamide is well suited for the use in a distillation test rig and for the operation with the standard reference systems, as the melting range is around $175\,°\mathrm{C}$ and there is a high chemical resistance to organic solvents [29]. Depending on the exact 3D printing material specification, it has been observed that residuals of the powder can accumulate in the reboiler during column operation. For this reason, it is advisable to infiltrate the 3D printed column components. Particularly advantageous for quick adaptation of the components is that they can be designed within a few seconds via the VBA plugin in Autodesk® Inventor using simple dimensioning parameter adaptation. This has been implemented for all 3D printed column components such as the column C1 and the multifunctional trays MFT1 and MFT2.

3.2.1 Multifunctional trays

The two multifunctional trays below (MFT1) and above the column C1 (MFT2) are available for connecting all 3D printed components with standard laboratory equipment. For this purpose, 3D printed connection types namely ground joints, small flanges and conventional flanges with flexible dimensions were implemented. In addition, threads were subsequently added after the printing process to allow threaded connections. The MFTs shown in Figure 2 thus allow connections with temperature and differential pressure sensors, as well as fluid inlets and outlets.

A standard ground joint is used to connect the reboiler HEx1 and the multifunctional tray MFT1. Good tightness was observed when using the 3D printed connection. Above the MFT1 is column C1, which can be connected vacuum-tight via small flanges from Leybold GmbH. The same connection can be observed at the lower connection of the MFT2. The upper connection of the MFT2 was adapted to the flange connection with a PTFE bellow, which is located below the condenser HEx2.

The internal design of both multifunctional trays is based on chimney trays. These are meant for collecting the liquid that trickles down. In the process, the gas generated in the reboiler HEx1 can flow upwards through relatively large recesses in the neck. Threads were cut into the 3D printed components to connect the nozzles with vacuum-tight screw joints from Bohlender GmbH. While in MFT1 the liquid flows back to HEx1 via the neck of the chimney, in the MFT2 it is fed into the distillate circuit via the upper right nozzle. The lower right nozzle, on the other hand, acts as a re-entry point for the liquid above the packing. The other nozzles are used for the introduction of Pt100 for temperature measurement (TIR02 and TIR03), as well as for the future planned measurement of differential pressure drops in the column. To measure the separation efficiency of the packing, it is important to be able to take samples directly above and below the packing, so that the calculated *HETP* value only refers to the

packing itself, without including the reboiler. While sampling of the MFT1 can be done directly at the right nozzle, sampling of the distillate is done in the distillate circuit, which is described in Section 3.3. The details of sampling and analytics are described in Section 3.4.

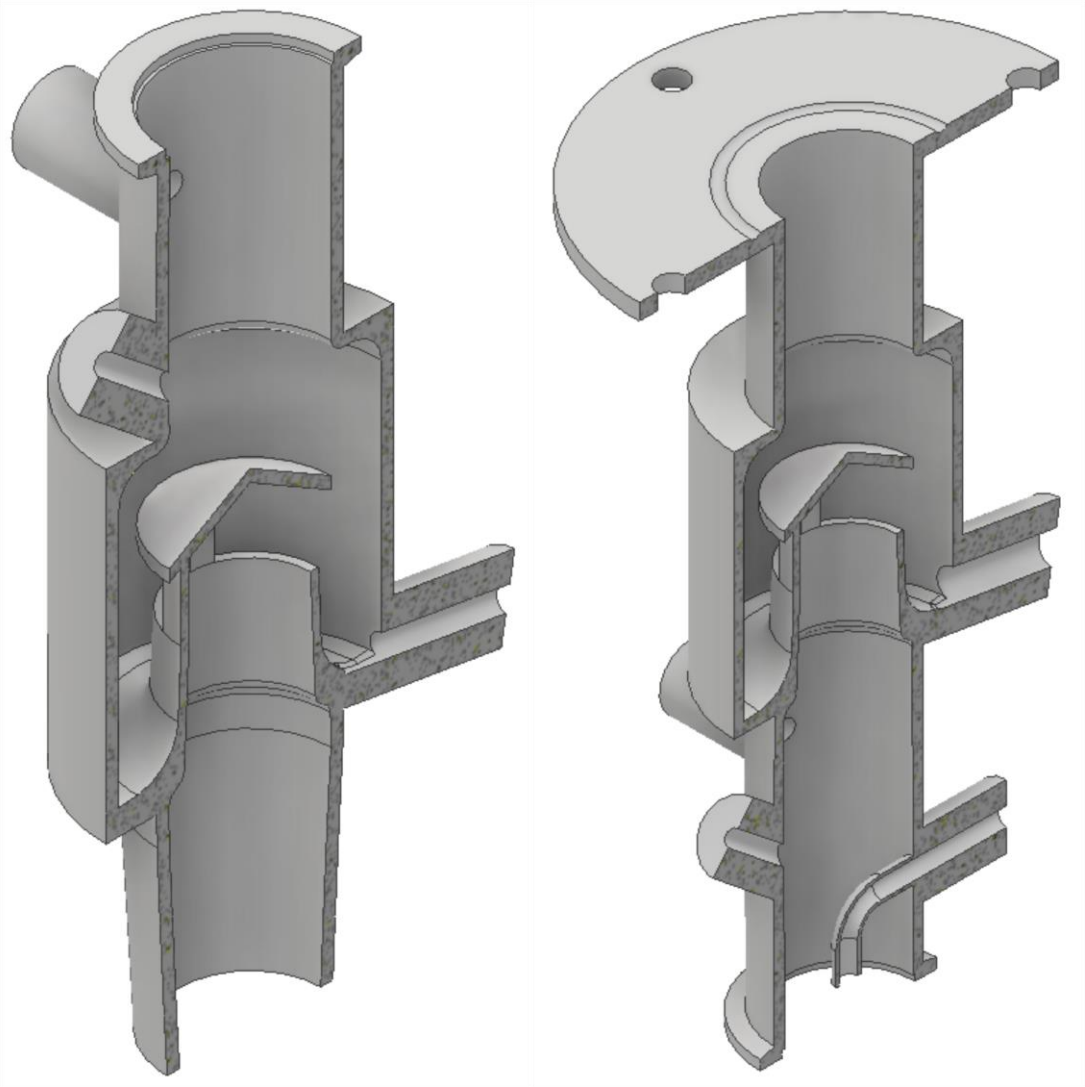

Figure 2: Multifunctional tray MFT1 right below the packing (left) and MFT2 right above the packing (right).

3.2.2 Column wall with packing

Just like the upper connection of the MFT1 and the lower connection of the MFT2, the additively manufactured column walls are also connected to each other with small flanges from Leybold GmbH. The diameters of the column wall can be continuously varied and automatically fitted with the appropriate small flange. The design using small flanges also allows the columns to be disassembled and reassembled quickly, making packing changes particularly

efficient. Currently, the column is insulated with two $13\,\mathrm{mm}$ thick layers of high temperature synthetic latex isolation (Armaflex HT). However, an optimized variant of the insulation is already being worked on.

An important focus in the development of miniaturized scalable distillation columns is on the development of novel packing structures to obtain constant and high separation efficiencies over a wide operating range. Several different packings have already been tested in this test rig. As an example, the procedure and implementation will be presented using a 3D printable version (RP9M 3D) of the original Rombopak 9M (RP9M) from Kühni/Sulzer [30]. For this purpose, the basic structure of the RP9M has been parameterized in a way that the crosspiece angle, the height of a unit cell, and the diameter and packing height can be changed quickly. The most important parameters of the RP9M 3D are shown in Table 1 and illustrated in Figure 3. The main differences to the original RP9M are, on the one hand, the significantly larger crosspiece thicknesses of $d = 0.8\,\mathrm{mm}$ (due to the minimum wall thickness for the SLS method) compared to the approximately $0.1\,\mathrm{mm}$ thick metal sheets of the original structure, and, on the other hand, that wall wipers were not included. Furthermore, the two structures differ in terms of their surface structure. While the original Rombopak 9M is profiled at certain intervals on the crosspieces, in the 3D printable variant (RP9M 3D), these are approximated by a sinusoidal profile.

Table 1: Packing parameters of the 3D printable version of the RP9M.

Parameter	**Value**
Height H_{UC} of one unit cell in mm	30
Broadness b of one crosspiece in mm	6
Thickness d of one crosspiece in mm	0.8
Crosspiece angle γ in °	45
Height k of the vertical connector in mm	3.5
Number n of sine waves on one crosspiece	5
Amplitude s of sine waves in mm	0.3

Packing diameter D_P in mm	50
Spec. geom. surface area $a_{geo,P}$ (only packing) in m^{-1}	358.4
Spec. geom. surface area $a_{geo,PW}$ (with wall) in m^{-1}	429.0
Void fraction ε in %	88.2

One packing element as shown in Figure 3 on the right consists of three layers stacked on top of each other. Accordingly, this is 9 cm high. A tongue and groove system allows packings to be accurately twisted by 90° from packing element to packing element. This approach is not limited to this structure. In addition, the lower ring of the lowest packing element can rest on a support ring in the column shell so that the packing does not slip through the column jacket. The maximum packing height in the plant is one meter, which is usually fully utilized (depending on the packing used).

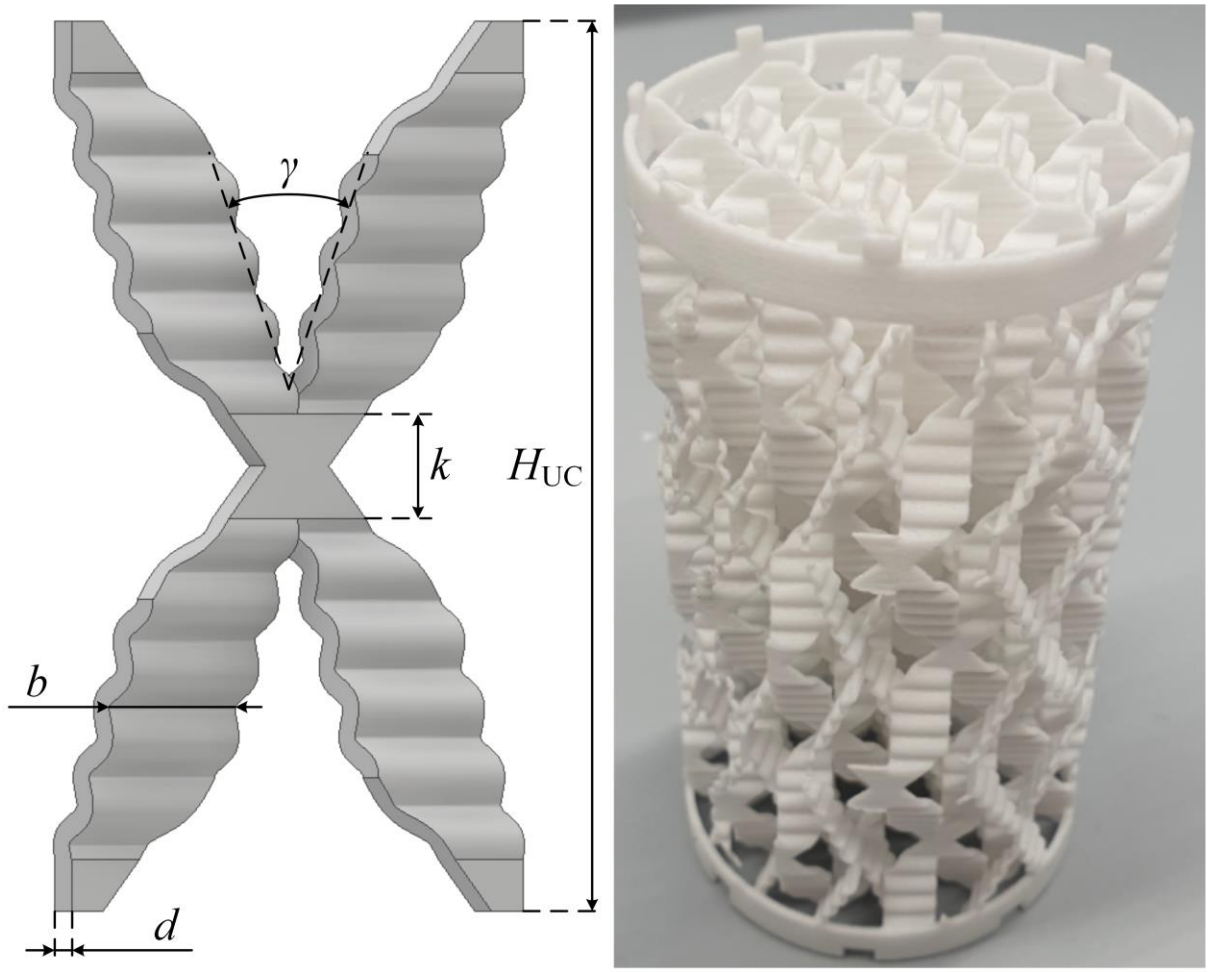

Figure 3: Illustration of the important RP9M 3D parameters (left) and photograph of the RP9M 3D (right).

3.3 Distillate circuit

The condensation of the rising steam takes place in the heat exchanger HEx2 manufactured by BASF SE, which is operated with cooling water at 18 °C. A heat exchange surface of $A = 0.48\,\mathrm{m}^2$ is provided in a confined space by a triple coil in an inclined design. The condensate enters the distillate circuit via the multifunctional tray (MFT2). The distillate then flows through the distillate container DC1, which was also manufactured at the BASF SE. To measure the level in the distillate container DC1, a float of the type TORRIX NT from the company Fafnir GmbH is used. The float itself is made of titanium and is suitable for liquids with a density of $\rho_\mathrm{L} > 500\,\frac{\mathrm{kg}}{\mathrm{m}^3}$. A constant level is set (LIRC01) in the distillate container DC1, via the gear pump P1 from the company Gather Industry GmbH. All signals are coordinated via the process control system in LabVIEW^{TM}. A sample from the distillate S03 can be taken between the gear pump P1 and the distillate container DC1 via the valve V05. Since the particularly wide operating range with variable column diameters between $D = 20\,\mathrm{mm}$ and $D = 50\,\mathrm{mm}$ also requires a large flow measuring range, a coriolis mass flow meter from Siemens is used. This has a measuring receptacle of the type SITRANS FC MASS2100 and a transmitter of the type SITRANS FCT030. In order to ensure the desired measuring range for *F*-factors of $F = 0.15\,\mathrm{Pa}^{0.5} \ldots 1.0\,\mathrm{Pa}^{0.5}$ for the variable column diameters mentioned above, it must be possible to measure volumetric flows between roughly $0.05\,\frac{\mathrm{l}}{\mathrm{h}}$ and $20\,\frac{\mathrm{l}}{\mathrm{h}}$. This corresponds to a ratio of $1/400$ from minimum to maximum distillate volume flow. This large operating range must also be able to be covered by the gear pump P1. The pump is capable of handling volume flows between $0.2\,\frac{\mathrm{l}}{\mathrm{h}}$ and $20\,\frac{\mathrm{l}}{\mathrm{h}}$. By using a bypass, which partially diverts the pumped liquid back into the distillate tank, less liquid is effectively fed into the column via the coriolis mass flow meter. Accordingly, the required liquid volume flow of $0.05\,\frac{\mathrm{l}}{\mathrm{h}}$ can be realized. The bypass flow can be manually adjusted via the shut-off valve V10 and the fine metering valve V11 so that the pump operates in an appropriate performance range.

The need for the gear pump and distillate container results from a relatively large pressure drop in the coriolis mass flow meter at higher flows. The hydrostatic pressure would not be sufficient to transport the distillate back to column C1 via the coriolis mass flow meter. In addition, it must be ensured that no cavitation occurs in the gear pump P1, as the distillate circuit initially has a temperature near the boiling point. For this reason, cooling water can flow around the HEx3 cooling tube and the double-walled distillate container DC1 or they can be bypassed. Directly before the distillate stream re-enters column C1, the degree of subcooling is measured with a Pt100 (TIR04). To be able to remove the liquid completely from the distillate circuit, the valves V6, V9, V14, V15 and V16 are available. The two valves V14 and V15 are used for venting so that the liquid can drain out of the lines. The check valve V8 provides a sufficiently large back pressure, which is necessary for proper pump operation.

3.4 Sampling and analytics

In the distillation test rig, liquid samples can be taken at the reboiler HEx1 (S01), below the packing at the multifunctional tray MFT1 (S02) and in the distillate circuit (S03). The sample in the distillate circuit has the same composition as the liquid directly above the column in the multifunctional tray MFT2. This ensures that only the packing without the impact of the re-boiler is considered in the separation efficiency calculations. Since the pilot plant is also to be operated under vacuum conditions in the future, sampling is carried out using gas-tight glass-PTFE syringes. When a sample is to be taken from the system, the syringe is coupled to the system via a Luer Lock connection and the corresponding valve V01, V04 or V05 is opened. The syringe is drawn up and the first two samples are initially placed in a beaker. Only the third sample is used for analysis so that the influence of dead volume is prevented as far as possible. Residues of 3D printing powder might accumulate in the evaporator, which is why the analysis injection is carried out via syringe filters with a pore size of 0.25 µm. After the analysis is performed, the residual liquid from the syringe and from the beaker is returned to

the system at the same sampling point. This ensures that only very small amounts of the mixtures are removed from the system and thus the equilibrium remains largely unaffected.

For the analysis the gas chromatograph GC-2030 ATF of the company Shimadzu with a semi polar column and a flame ionization detector is used. However, for fast analyses, a A.Krüss Optronic GmbH refractometer of the type DR6300-T is also used if necessary. Accuracy studies showed that when using the GC with the deposited calibration curve, relative errors of less than 2% can be expected. With the refractometer and the deposited calibration curve, on the other hand, errors $< 5\%$ are observed. For both methods, the error becomes more pronounced in the diluted edge regions.

4 Pilot plant operation results

Prior to operation of the plant, about 2.5l of the system cHex/nHep are prepared with a molar fraction of the light boiling cHex of 10%. After the plant has been filled with the mixture, it is inertized with nitrogen. The plant is then ready for operation. The results presented in the following sections all refer to an operation of the plant with a column diameter of $D = 50\,\mathrm{mm}$ and atmospheric conditions.

4.1 Stability and performance tests

Figure 4 shows typical curves of important key parameters with regard to the stability and performance of the plant. In order to approach different operating points of the plant, the duty of the reboiler HEx1, shown as a dashed line, is specified. The gear pump adjusts the duty, shown as a light gray solid line, so that the specified liquid level in the distillate container DC1, shown as a dotted line, of 10% is set. While the resulting mass flow, measured in the coriolis mass flow meter FIR01, illustrated as black solid line, is assigned on the left side in Figure 4, all other parameters are assigned to the scale on the right.

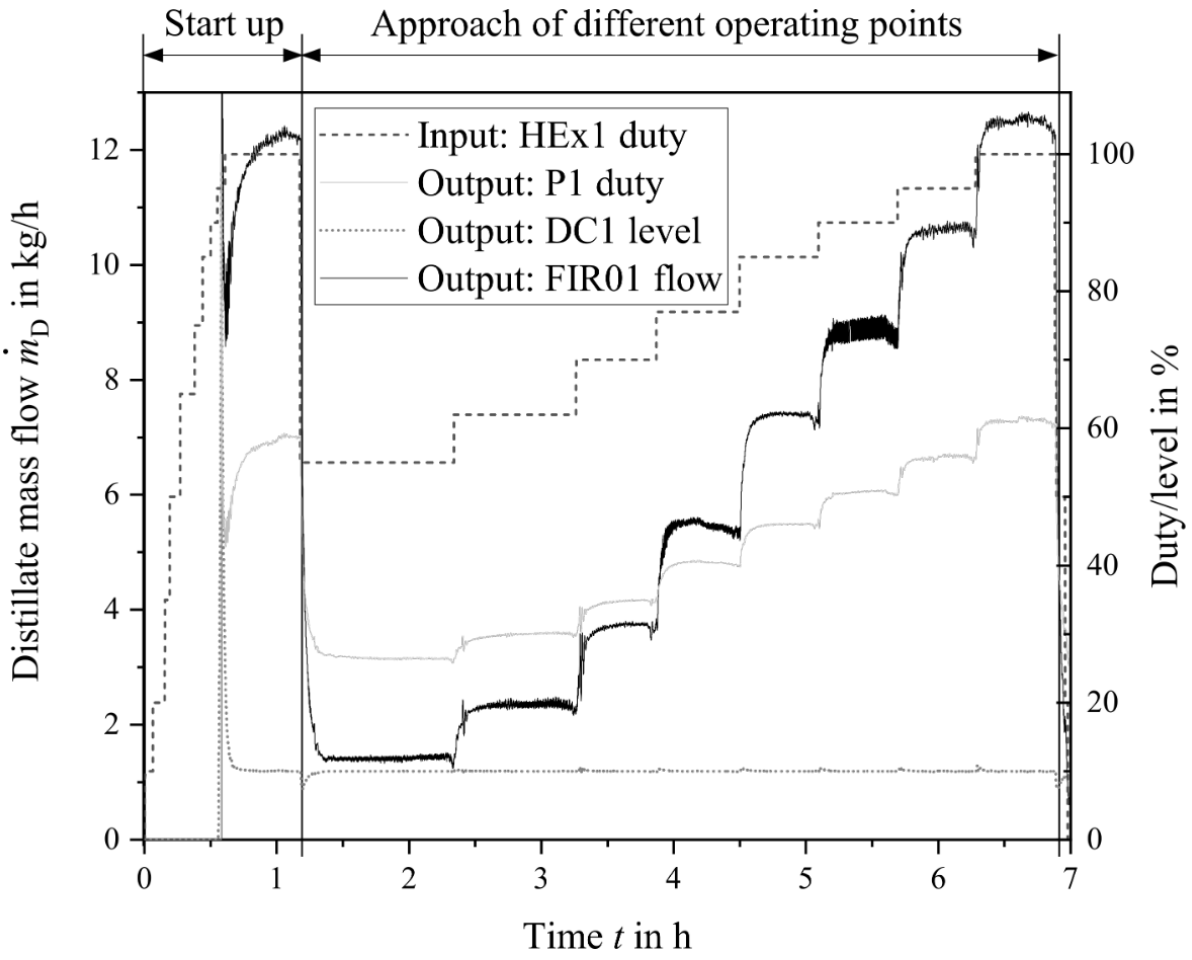

Figure 4: Illustration of key parameters regarding the operational stability of the plant, exemplified by a typical plant operation program to determine the separation efficiency of a packing.

The left part of Figure 4 shows the start-up of the plant. To the right of this, various operating points were approached. The shutdown is indicated on the far right, but data logging is usually already aborted here and this process is completed quickly. The start-up of the column takes about one hour. First, the power in the reboiler HEx1 is increased step by step. This process should not be carried out too quickly, otherwise there is a risk that the heating rods, consisting of quartz glass, will crack due to too rapid heating. Over a period of 30 minutes, the system fills with gas until finally the first distillate droplets are formed and the distillate container DC1 gradually fills with liquid. Once a certain liquid level has been reached in the distillate container DC1, the gear pump P1 is switched on, which in turn regulates the liquid level to the specified set point of 10%. Only now can the distillate mass flow be registered by the flow

meter FIR01. To ensure that the initial conditions in the system are always the same, it is initially operated at a reboiler duty of 100 % for a period of about 30 min, so that the entire packing installed can be wetted. The indicated plateau in the course of the distillate mass flow and the gear pump duty, as well as a constant liquid level in the distillate container DC1 mark the end of the start-up phase.

Now, the operating point for the lowest liquid and gas load is set by reducing the reboiler duty. After an approximately constant plateau has been established for all key parameters from Figure 4, it is assumed, that a steady-state behavior is reached. A more detailed consideration of when steady-state conditions are reached is discussed in Section 4.2. The sample is then analyzed in the GC. Finally, the liquid in the beakers is injected back into the system at the same location where the sample was taken so that the equilibrium is affected as little as possible by the sampling. During this process, slight fluctuations in the liquid level of the distillate container DC1 can be observed in Figure 4. Within a few seconds, however, the level is adjusted to almost exactly 10 % liquid level. During steady-state operation, the fluctuations amounted to ±0.02 % in the liquid level. In addition, very low oscillating operating points can occur (see Figure 4 at a time of 5.5 hours), which are mainly reflected in the measured mass flow. Since the liquid level in the distillate container DC1 is constant at 10 %, the error can be largely excluded by averaging all measured values over a certain period of time. Now, the next operating point can be approached by increasing the reboiler capacity. This procedure is repeated until the desired operating range has been covered. The pilot plant can then be shut down.

4.2 Steady-state test

This section examines at what point the assumption of steady-state operation is considered justified. To ensure stationary conditions in the plant, the liquid in the distillate circuit and in the column must be renewed several times. The residence time is an important key parameter with regard to achieving steady-state conditions. Since the holdup in the plant can only be

estimated very roughly, a steady-state test can provide clarity. For this purpose the packing is wetted as well as possible by setting the maximum reboiler duty, as described in Section 4.1. Afterwards, other operating points can be approached. As an example, Figure 5 shows the trend of the *HETP* value over a period of 4 hours exemplary for two different packings at two different operating points. After the start-up phase with complete wetting of the packing, a random steady-state operating point was set. After sampling at this point, the reboiler duty was adjusted at time $t = 0$ min resulting in an *F*-factor of $F = 0.34 \pm 0.06\,\mathrm{Pa}^{0.5}$ for packing 1 and $F = 0.09 \pm 0.02\,\mathrm{Pa}^{0.5}$ for packing 2, calculated according to Equation (2.7). During 4 hours of plant operation, analytical samples were collected at times $t = 0\,\mathrm{min}$, $t = 10\,\mathrm{min}$, $t = 20\,\mathrm{min}$, $t = 60\,\mathrm{min}$, $t = 120\,\mathrm{min}$, $t = 240\,\mathrm{min}$. Regarding the *HETP* value trend, one notices that the values for the first packing at the moderate *F*-factor do not change significantly after a time period of 30 minutes. The second packing, on the other hand, shows a slightly decreasing *HETP* value over the time interval. As expected, it was found that at lower gas loads, it is necessary to wait longer in order to reach steady-state conditions. This results from a significantly increased residence time of the liquids in the distillate circuit. Accordingly, in the range of very low *F*-factors a correspondingly longer time is waited before sampling. The exact idle time depends on how low the gas load is and how accurate the result should be. However, a time of 30 minutes is set as the minimum idle time before a steady-state operating point is assumed. The course shown in Figure 4 reflects this procedure. Accordingly, the first sample was taken after a waiting time of $1\,\mathrm{h}$, the second after a waiting time of $45\,\mathrm{min}$ and all further samples after $30\,\mathrm{min}$ in this specific example. To evaluate the results presented, the error bars are illustrated in this section. More detailed information on the error calculation can be found in the following section or in Appendix 7.2.

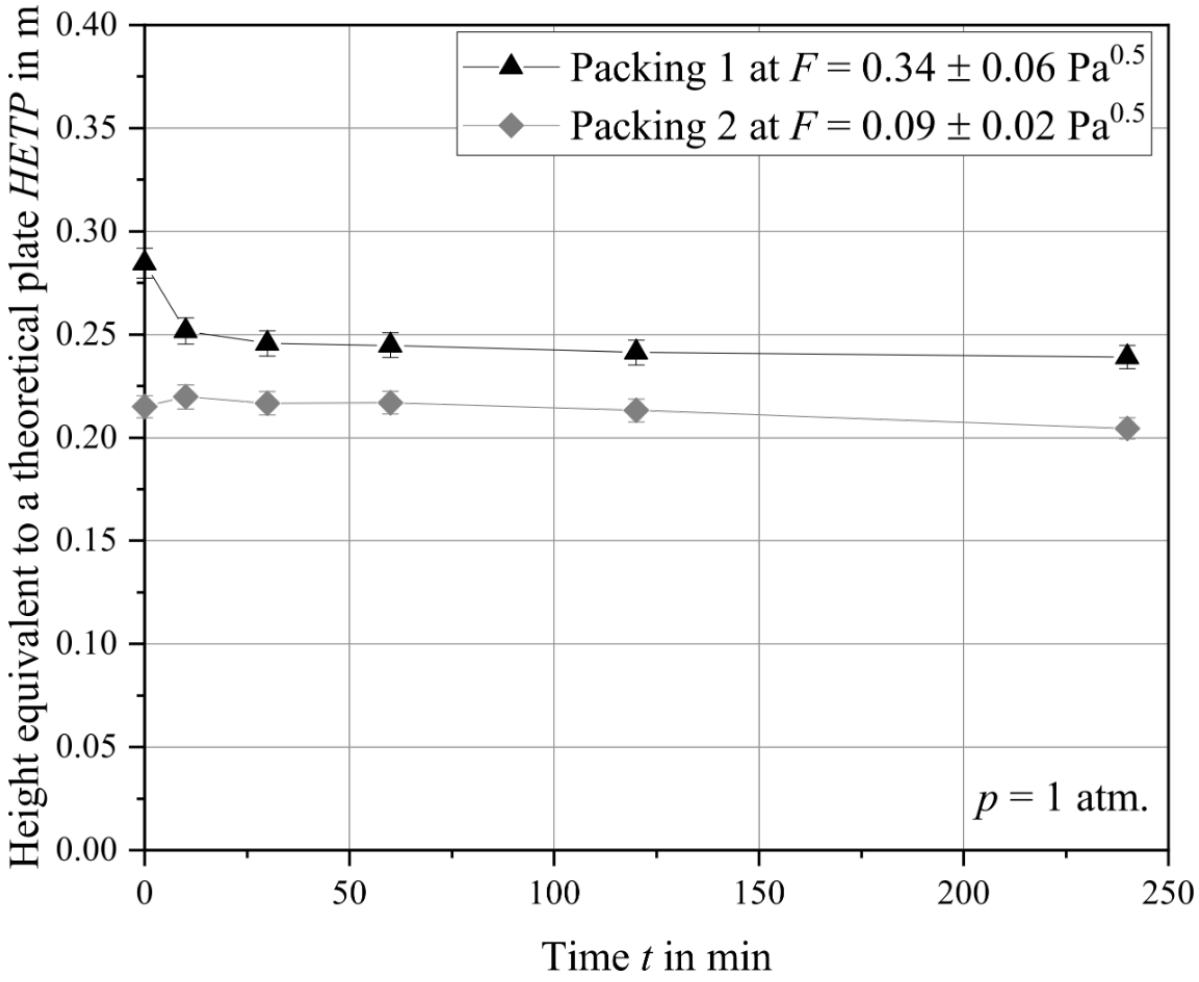

Figure 5: Trend of the *HETP* value of packing 1 and packing 2 over a four hour period.

A suitable operating mode could be identified for operation at a column diameter of $D = 50\,\text{mm}$. For operation at smaller column diameters and fundamentally different packings, new stationarity tests should be performed accordingly to ensure the accuracy of the measurements. Subsequently, the waiting times until stationary operating conditions are reached must be adjusted accordingly.

4.3 Mass transfer measurements

The separation efficiency of the measured packing shall be described in this section with the *HETP* value, which was obtained at a certain gas load in steady-state. Here, the average *F*-factor was calculated according to Equation (2.7). This equation corresponds to an averaging over the two extreme states above and below the packing. The gas mass flow above the packing $\dot{m}_G^T$ corresponds to the mass flow measured in the distillate circuit. The mass flow rate below the

packing $\dot{m}_G^B$ is calculated according to Equation (2.6) in Section 2. Due to the small packed height of one meter, the pressure drop was assumed to be negligible (below 10 mbar). Corresponding pure parameters like heat of evaporation Δh_V, liquid heat capacities $c_{p,L}$ and the molar mass M as well as with the approaches to calculate the respective values of the mixtures have been gathered in Equations (A.2), (A.3), (A.5) and (A.6) in Appendix 7.1. Relevant measured variables for the calculations are, on the one hand, the mass flow in the distillate circuit (FIR01) and, on the other hand, the temperatures at the sampling points and in the distillate circuit directly before re-entry into the column (TIR01, TIR02, TIR03 and TIR04). These quantities were averaged over a certain period of time after reaching a largely steady-state operating point according to Section 4.2.

Figure 6 shows an example of the *HETP* value of the 3D printable Rombopak version RP9M 3D plotted against the *F*-factor. To calculate the error bars shown here and also in Figure 5, the error propagation law was applied to Equation (2.1) and Equation (2.11) combined with Equation (2.8). For this purpose, the standard deviation was used as the error for gas densities, the gas mass flow and the relative volatility. For the measurement errors during determination of the mass fractions of the components in the GC, an error of 2% was assumed.

The relatively large errors of the *F*-factor can be described using the error calculation in Appendix 7.2. The averaged *F*-factor is determined by the average mass flow and the average gas density above and below the packing. Higher subcooling of the reflux stream in the distillate circuit makes the discrepancies at the top and bottom more pronounced. For smaller *F*-factors, the absolute error is smaller than for high *F*-factors, despite greater subcooling. This results from the significantly smaller reflux mass flow that has to be brought back to boiling temperature in the column. Depending on the operating point, the degree of subcooling is around 20 K for high *F*-factors and around 45 K for very small *F*-factors. The differences in the internal

mass flows due to heat losses via the column wall are not yet taken into account in the error calculation.

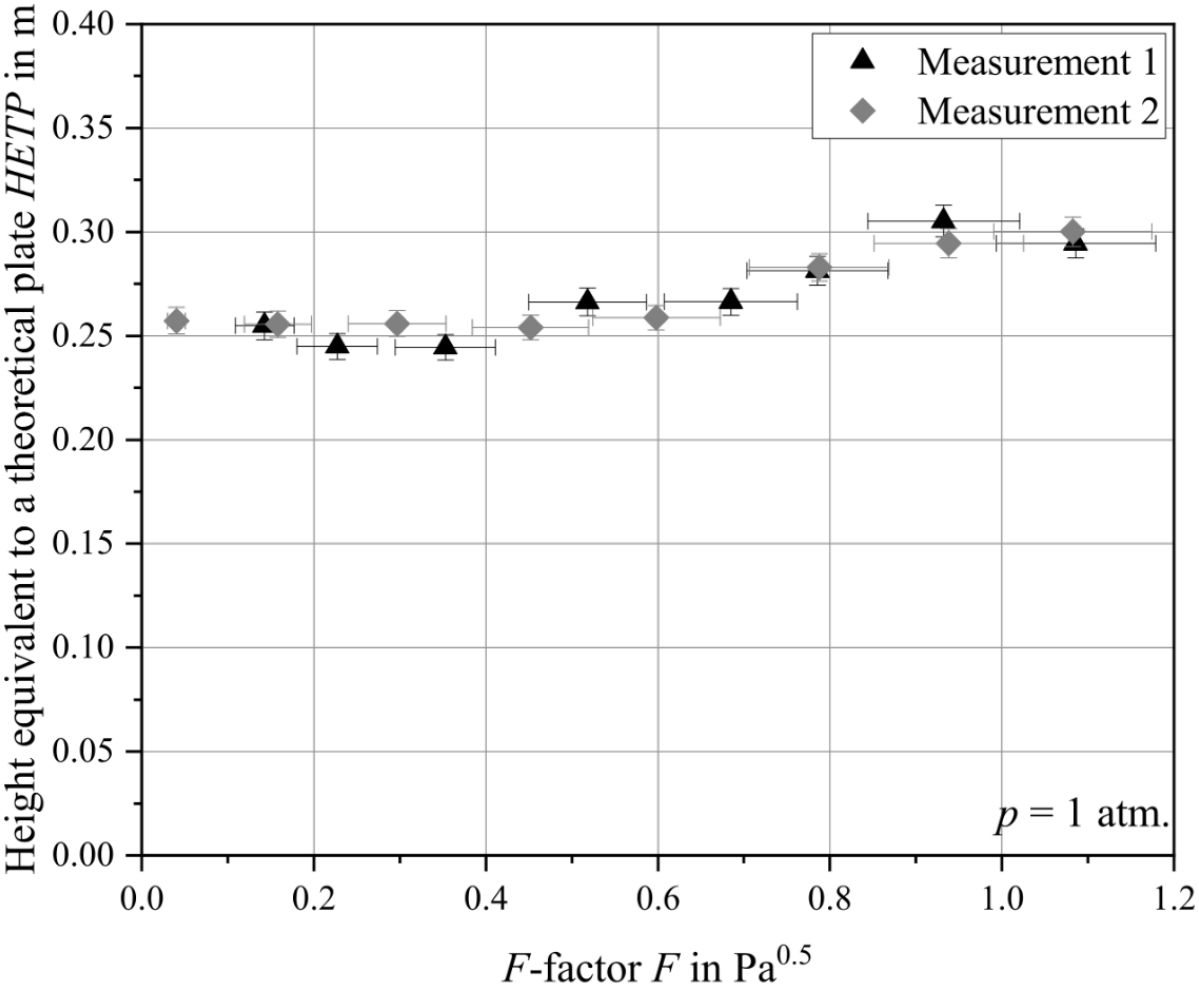

Figure 6: Separation efficiency of the 3D printable version of the Rombopak 9M.

When comparing both series of measurements shown in Figure 6, it becomes clear that a realistically good agreement and reproducibility of the results can already be achieved. The original Rombopak 9M has a decreasing separation performance in the considered operating range. This trend was also observed for the 3D printable version of the Rombopak. [31] In general, however, the separation performance was significantly lower compared to literature data. This could be due to the lack of wall wipers, the fact that the replica is not perfectly true to the original and that data was only found for the system chlorobenzene/ethylbenzene for the RP9M.

5 Summary and outlook

Due to the increasing application fields of additive manufacturing, many new design approaches for packings in the field of thermal separation technology as outlined in Section 1 are presented in the literature. This contribution focuses on the experimental setup of one of the first distillation columns for characterizing additively manufactured packings. The test facility is characterized by a particularly wide operating range. This enables the characterization of additively manufactured packings with diameters between $D = 20\,\mathrm{mm}$ and $D = 50\,\mathrm{mm}$. Gas loads of at least $F = 1\,\mathrm{Pa}^{0.5}$ can be achieved for all column diameters, which covers the standard operating range of laboratory columns. The experimental plant exhibits remarkably stable operation and also reaches steady-state correspondingly quickly. However, the smaller the internal mass flows get, the longer the time until stationarity is reached. The investigations were presented as an example using a 3D printable version of the Rombopak 9M developed by Kühni/Sulzer [30]. By parameterizing all structures, a wide variety of packings can be created within a few seconds using the VBA plug-in in Autodesk® Inventor. The packings are additively manufactured from PA12 rather than metal, mainly for cost reasons. They can be accurately inserted into the column jacket, which is also 3D printed. Two additively manufactured multifunctional trays were also presented, which function as sampling points, for diverting the distillate stream, or as connection points to various measurement sensors. All these 3D printed components are either coupled with each other or with conventional laboratory equipment via standard connection systems, such as ground joints, flanges, small flanges and threads.

However, the overall goal of the project is to reduce the packing diameter as much as possible while maintaining scalability to industrial scale columns. Scalability problems are mainly caused by increasing wall-to-core ratios in the column at reduced diameters. Accordingly, new types of packings are currently also being developed with the aid of CFD simulations, among

other things, which have the best possible fluid distribution, are characterized by high separation efficiency and still have an acceptable pressure drop. More detailed investigations will then be carried out in experimental plants at the Technical University of Munich and in the distillation test rig presented in this paper at Ulm University. To achieve even better results, the addition of a further heat exchanger for distillate preheating before reentry into the column is already on the agenda. In addition, the test plant is to be supplemented by the necessary measuring equipment so that the pressure drop of the packings can also be determined experimentally. In order to be able to carry out a further reproducibility study, vacuum operation down to 25 mbar is also to be made possible. Currently, various packings have already been investigated at diameters of 50 mm. The experimental setup is also designed for studies at smaller column diameters. However, these measurements have not been conducted yet.

Latin symbols

A	$[\mathrm{m^2}]$	area
a	$[\mathrm{m^2\,m^{-3}}]$	specific surface area
B	$[\mathrm{m^3\,m^{-2}\,h^{-1}}]$	liquid load
b	$[\mathrm{mm}]$	crosspiece broadness
c	$[\mathrm{J\,kg^{-1}\,K^{-1}}]$	specific heat capacity
D	$[\mathrm{m}]$	diameter
d	$[\mathrm{mm}]$	crosspiece thickness
F	$[\mathrm{Pa^{0.5}}]$	F-factor
H	$[\mathrm{m}]$	height
$HETP$	$[\mathrm{m}]$	height equivalent to a theoretical plate
h	$[\mathrm{J\,kg^{-1}}]$	specific enthalpy
k	$[\mathrm{mm}]$	vertical crosspiece connection height
M	$[\mathrm{g\,mol^{-1}}]$	molar mass
m	$[-]$	number of supporting points
$\dot{m}$	$[\mathrm{kg\,s^{-1}}]$	mass flow
N	$[-]$	number of stages
$NTSM$	$[\mathrm{m^{-1}}]$	number of theoretical stages per meter packed height
n	$[-]$	number of sine waves on a crosspiece
p	$[\mathrm{Pa}]$	pressure
R	$[\mathrm{J\,mol^{-1}\,K^{-1}}]$	ideal gas constant
T	$[\mathrm{K}]$	temperature
u	$[\mathrm{m\,s^{-1}}]$	velocity
w	$[-]$	mass fraction
x	$[-]$	molar fraction of the liquid phase
y	$[-]$	molar fraction of the gas phase

Greek symbols

α	$[-]$	relative volatility
γ	$[^\circ]$	crosspiece angle

ε	$[-]$	void fraction
ρ	$[\mathrm{kg\,m^{-3}}]$	density

Indices

avg	averaged
B	bottom
C	column
c	critical
cHex	cyclohexane
G	gas
geo	geometric
i	run variable
L	liquid
nHep	*n*-heptane
P	packing
PW	packing with column wall
p	constant pressure
R	reflux
T	top
th	theoretical
UC	unit cell
V	evaporation

Abbreviations

CAD	computer aided design
CFD	computational fluid dynamics
cHex	cyclohexane

nHep	*n*-heptane
PA12	polyamide 12
P&ID	piping and instrumentation diagram
RP9M	Rombopak 9M
RP9M 3D	3D printable version of the Rombopak 9M
SLS	selective laser sintering

6 References

[1] J.G. Stichlmair, J.R. Fair, Distillation: Principles and practices, Wiley-VCH, New York, 1998.

[2] F. Hanusch, S. Rehfeldt, H. Klein, Liquid Maldistribution in Random-Packed Columns: Experimental Investigation of Influencing Factors, Chem. Eng. Technol. 41 (2018) 2241–2249. https://doi.org/10.1002/ceat.201800467.

[3] K. Fent, Ökotoxikologie: Umweltchemie, Toxikologie, Ökologie, fourth., vollständig überarbeitete Auflage, Thieme, Stuttgart, 2013.

[4] E. Grossman, Chasing molecules: Poisonous products, human health, and the promise of green chemistry, 2009.

[5] United States Government Accountability Office, Report to Congressional Requesters, Toxic Substances - EPA has increased efforts to assess and control chemicals but could strengthen its approach, 2013.

[6] L. Deibele, R. Dohrn, Miniplant-Technik in der Prozessindustrie, first. Aufl., Wiley-VCH, Weinheim, 2006.

[7] W. Hofen, M. Körfer, K. Zetzmann, Scale-up-Probleme bei der experimentellen Verfahrensentwicklung, Chemie Ingenieur Technik 62 (1990) 805–812. https://doi.org/10.1002/cite.330621006.

[8] A. Gebhardt, J. Kessler, L. Thurn (Eds.), 3D-Drucken, Carl Hanser Verlag GmbH & Co. KG, München, 2016.

[9] C. Hurt, M. Brandt, S.S. Priya, T. Bhatelia, J. Patel, P. Selvakannan, S. Bhargava, Combining additive manufacturing and catalysis: a review, Catal. Sci. Technol. 7 (2017) 3421–3439. https://doi.org/10.1039/c7cy00615b.

[10] C. Parra-Cabrera, C. Achille, S. Kuhn, R. Ameloot, 3D printing in chemical engineering and catalytic technology: structured catalysts, mixers and reactors, Chem. Soc. Rev. 47 (2018) 209–230. https://doi.org/10.1039/c7cs00631d.

[11] F. Kotz, P. Risch, D. Helmer, B.E. Rapp, High-Performance Materials for 3D Printing in Chemical Synthesis Applications, Adv. Mater. 31 (2019) e1805982. https://doi.org/10.1002/adma.201805982.

[12] A. Lange, G. Fieg, Shape optimization of additively manufactured structured packings for distillation columns, poster at CHISA online conference, 2021.

[13] B. Dejean, M. Meyer, D. Rouzineau, Design and conception of an innovative packing for separation column—Part I: Hydrodynamic study on wire intersections, Chemical Engineering Research and Design 160 (2020) 11–19. https://doi.org/10.1016/j.cherd.2020.05.006.

[14] A. Zimmer, J.D. PachecoAraújo, K.A. Andreassen, C.A. Grande, Effect of Manufacturing Techniques in Pressure Drop on Triple Periodical Minimal Surface Packings, Chemie Ingenieur Technik (2021). https://doi.org/10.1002/cite.202000237.

[15] K. Gładyszewski, M. Skiborowski, Additive manufacturing of packings for rotating packed beds, Chemical Engineering and Processing - Process Intensification 127 (2018) 1–9. https://doi.org/10.1016/j.cep.2018.02.024.

[16] H. Qammar, K. Gładyszewski, A. Górak, M. Skiborowski, Towards the Development of Advanced Packing Design for Distillation in Rotating Packed Beds, Chemie Ingenieur Technik 91 (2019) 1663–1673. https://doi.org/10.1002/cite.201900053.

[17] Z.-N. Wen, W. Wu, Y. Luo, L.-L. Zhang, B.-C. Sun, G.-W. Chu, Novel Wire Mesh Packing with Controllable Cross-Sectional Area in a Rotating Packed Bed: Mass Transfer Studies, Ind. Eng. Chem. Res. 59 (2020) 16043–16051. https://doi.org/10.1021/acs.iecr.0c01886.

[18] S. Bolton, A. Kasturi, S. Palko, C. Lai, L. Love, J. Parks, S. Xin, C. Tsouris, 3D printed structures for optimized carbon capture technology in packed bed columns, Separation Science and Technology 54 (2019) 2047–2058. https://doi.org/10.1080/01496395.2019.1622566.

[19] F. Grinschek, D. Xie, M. Klumpp, M. Kraut, E. Hansjosten, R. Dittmeyer, Regular Microstructured Elements for Intensification of Gas–Liquid Contacting Made by Selective Laser Melting, Ind. Eng. Chem. Res. 59 (2020) 3736–3743. https://doi.org/10.1021/acs.iecr.9b04548.

[20] D. Zhang, J. Xiao, Q. Guo, J. Yang, 3D-printed highly porous and reusable chitosan monoliths for Cu(II) removal, J Mater Sci 54 (2019) 6728–6741. https://doi.org/10.1007/s10853-019-03332-y.

[21] A. Reitze, M. Grünewald, J. Riese, Experimentelle Untersuchung additiv gefertigter strukturierter Packungen für Laborkolonnen, Chemie Ingenieur Technik 92 (2020) 1304–1305. https://doi.org/10.1002/cite.202055220.

[22] J.E. Bara, C.I. Hawkins, D.T. Neuberger, S.W. Poppell, 3D printing for CO 2 capture and chemical engineering design, Nanomaterials and Energy 2 (2013) 235–243. https://doi.org/10.1680/nme/13.00021.

[23] S. Mardani, L.S. Ojala, P. Uusi-Kyyny, V. Alopaeus, Development of a unique modular distillation column using 3D printing, Chemical Engineering and Processing - Process Intensification 109 (2016) 136–148. https://doi.org/10.1016/j.cep.2016.09.001.

[24] J. Neukäufer, F. Hanusch, M. Kutscherauer, S. Rehfeldt, H. Klein, T. Grützner, Methodology for the Development of Additively Manufactured Packings in Thermal Separation Technology, Chem. Eng. Technol. 42 (2019) 1970–1977. https://doi.org/10.1002/ceat.201900220.

[25] M. Ottenbacher, Ž. Olujić, T. Adrian, M. Jödecke, C. Großmann, Structured packing efficiency—Vital information for the chemical industry, Chemical Engineering Research and Design 89 (2011) 1427–1433. https://doi.org/10.1016/j.cherd.2011.02.012.

[26] U. Onken, Recommended test mixtures for distillation columns, second. ed., The Institution of Chemical Engineers, Rugby, Warwickshire, 1990.

[27] E.J. Henley, J.D. Seader, D.K. Roper, Separation process principles, third. ed., internat. student version, Wiley, Hoboken, NJ, 2011.

[28] M.R. Fenske, Fractionation of Straight-Run Pennsylvania Gasoline, Ind. Eng. Chem. 24 (1932) 482–485. https://doi.org/10.1021/ie50269a003.

[29] G.W. Ehrenstein, S. Pongratz, Beständigkeit von Kunststoffen, Hanser, München, 2007.

[30] U.D.M.I. Buhlmann (KUEHNI AG [CH]) EP0069241 (A1), 1982.

[31] H.E. Steude, L. Deibele, J. Schröter, MINIPLANT -Technik - ausgewählte Aspekte der apparativen Gestaltung, Chemie Ingenieur Technik 69 (1997) 623–631. https://doi.org/10.1002/cite.330690504.

[32] VDI-Wärmeatlas, Springer, Berlin, Heidelberg, 2013.

7 Appendix A

7.1 Physical properties

The equations for the calculation of the pure component physical properties of nHep and cHex are given in Table A.1.

Table A.1: Pure component correlation equations [32].

Physical property	**Unit**	**Correlation equation**	**Eq.**
Liquid density	$\frac{\mathrm{kg}}{\mathrm{m}^3}$	$\rho_{\mathrm{L}} = \rho_{\mathrm{c}} + A\cdot\left(1-\frac{T}{T_{\mathrm{c}}}\right)^{0.35} + B\cdot\left(1-\frac{T}{T_{\mathrm{c}}}\right)^{\frac{2}{3}} + C\cdot\left(1-\frac{T}{T_{\mathrm{c}}}\right) + D\cdot\left(1-\frac{T}{T_{\mathrm{c}}}\right)^{\frac{4}{3}}$	(A.1)
Specific heat of vaporization	$\frac{\mathrm{kJ}}{\mathrm{kg}}$	$\Delta h_{\mathrm{V}} = R\cdot T_{\mathrm{c}}\cdot\left[A\cdot\left(1-\frac{T}{T_{\mathrm{c}}}\right)^{\frac{1}{3}} + B\cdot\left(1-\frac{T}{T_{\mathrm{c}}}\right)^{\frac{2}{3}} + C\cdot\left(1-\frac{T}{T_{\mathrm{c}}}\right) + D\cdot\left(1-\frac{T}{T_{\mathrm{c}}}\right)^{2} + E\cdot\left(1-\frac{T}{T_{\mathrm{c}}}\right)^{6}\right]$	(A.2)
Specific heat capacity of the liquid	$\frac{\mathrm{kJ}}{\mathrm{kg}\cdot\mathrm{K}}$	$c_{\mathrm{p,L}} = R\cdot\left[\frac{A}{1-\frac{T}{T_{\mathrm{c}}}} + B + C\cdot\left(1-\frac{T}{T_{\mathrm{c}}}\right) + D\cdot\left(1-\frac{T}{T_{\mathrm{c}}}\right)^{2} + E\cdot\left(1-\frac{T}{T_{\mathrm{c}}}\right)^{3} + F\cdot\left(1-\frac{T}{T_{\mathrm{c}}}\right)^{4}\right]$	(A.3)

The parameters for the correlation equation in Table A.1 for both components nHep and cHex are listed in Table A.2.

Table A.2: Parameters for the calculation of the pure component properties with the correlation equations in Table A.1 [32].

Physical property	**Parameter**	**nHep**	**cHex**
Molar mass of component j	M_j in $\frac{\text{g}}{\text{mol}}$	100.21	84.16
Critical density of component j	$\rho_{\text{c},j}$ in $\frac{\text{kg}}{\text{m}^3}$	225	273
Critical temperature of component j	$T_{\text{c},j}$ in K	540.3	553.8
Liquid density of component j	A	308.4582	373.9221
	B	1071.686	848.7461
	C	-1664.6321	-1261.1653
	D	990.254	815.8631
Specific heat of evaporation of component j	A	3.33801	3.43321
	B	21.88936	14.08811
	C	-18.680507	-8.768835
	D	5.467222	0.700818
	E	-2.994395	-0.075958
Specific liquid heat capacity of component j	A	0.6767	0.4835
	B	34.8802	28.0569
	C	-9.4333	-6.7431
	D	-51.0547	-118.2361
	E	57.7955	355.2759
	F	-1.9863	-383.5819

The properties of the mixtures were calculated using the mixing rules given in Table A.3. In the process, the excess contributions were neglected.

Table A.3: Mixing rules for the calculation of the physical properties of the mixtures [32].

Physical property	**Unit**	**Mixing rule**	**Eq.**
Liquid density of the mixture	$\frac{\mathrm{kg}}{\mathrm{m}^3}$	$\rho_L = \sum_j w_j \cdot \rho_{L,j}$	(A.4)
Specific heat of vaporization of the mixture	$\frac{\mathrm{kJ}}{\mathrm{kg}}$	$\Delta h_\mathrm{V} = \sum_j w_j \cdot \Delta h_{\mathrm{V},j}$	(A.5)
Specific liquid heat capacity of the mixture	$\frac{\mathrm{kJ}}{\mathrm{kg}\cdot\mathrm{K}}$	$c_{\mathrm{p,L}} = \sum_j w_j \cdot c_{\mathrm{p,L},j}$	(A.6)

The equilibrium data in order to calculate the relative volatilities was calculated by a polynomial trend line for the experimental data found in the Dortmund Data Bank from Onken et al. at ambient conditions [26], as shown in Figure A.1. The polynomial fit to the experimental data is described in Equation (A.7).

$$y_{\mathrm{cHex}} = 0.232007 \cdot x_{\mathrm{cHex}}^3 - 0.864233 \cdot x_{\mathrm{cHex}}^2 + 1.633216 \cdot x_{\mathrm{cHex}} \tag{A.7}$$

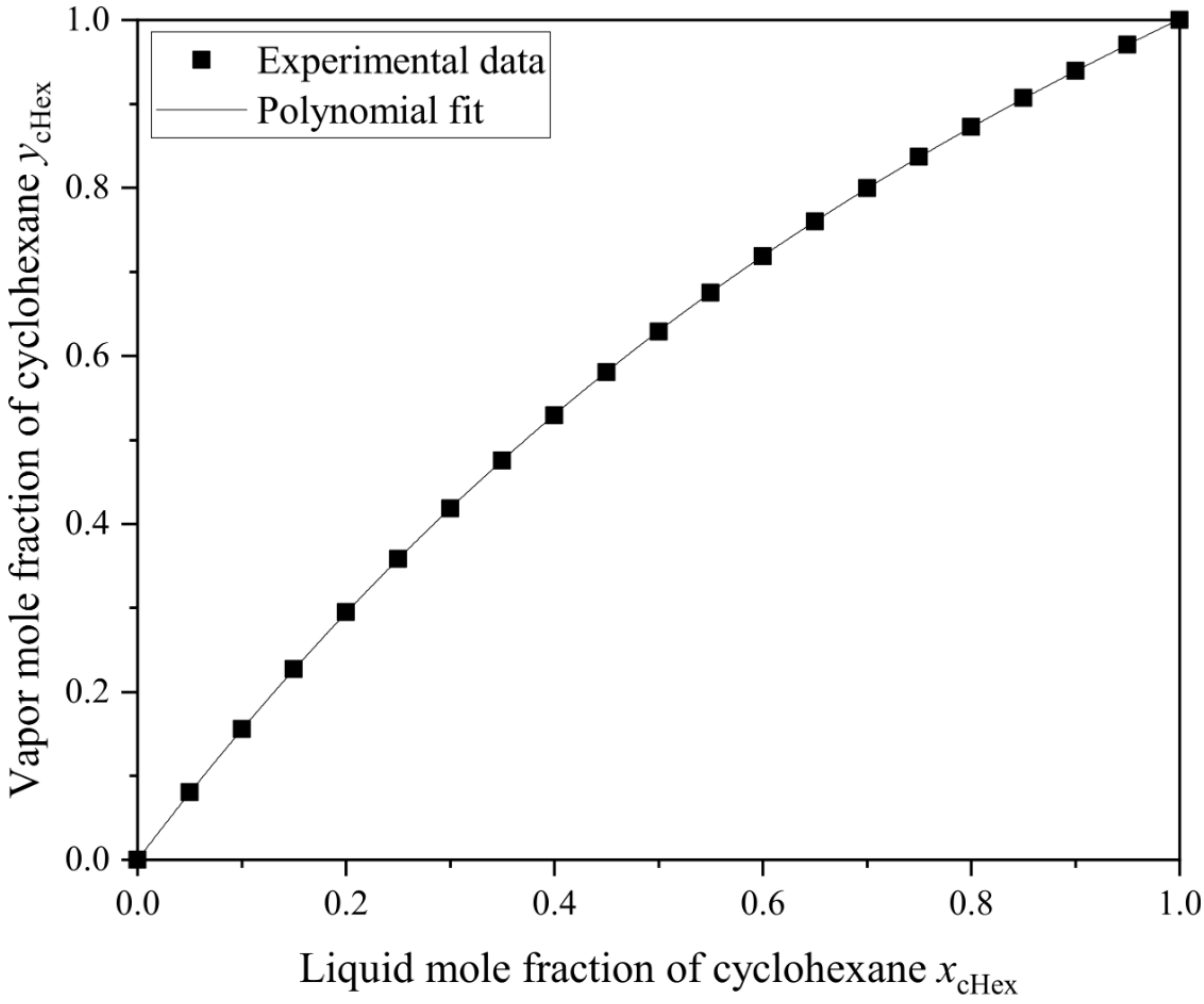

Figure A.1: Experimental equilibrium data from Onken et al. [26] with polynomial fit for the system cHex/nHep.

7.2 Error Analysis

F-factors and *HETP* values averaged over the packing were calculated using error propagation. In the equations for the error propagation, the standard deviations were used for the average gas density error and the average gas mass flow error. For the component molar fractions of cHex errors of 2% were assumed for every case.

The error for the average *F*-factor according to Equation (A.9) was calculated on the basis of equation (A.8).

$$F_{\text{avg}} = u_{\text{G,Avg}} \cdot \rho_{\text{G,avg}}^{0.5} = \frac{\dot{m}_{\text{G,avg}}}{\rho_{\text{G,avg}}^{0.5} \cdot A_{\text{C}}} \tag{A.8}$$

$$\Delta F_{\text{avg}} = \left(\left(\frac{\Delta \dot{m}_{\text{G,avg}}}{A_{\text{C}} \cdot \rho_{\text{G,avg}}^{0.5}} \right)^2 + \left(\frac{\left(-0.5 \cdot \dot{m}_{\text{G,avg}}\right) \cdot \Delta \rho_{\text{G,avg}}}{A_{\text{C}} \cdot \rho_{\text{G,avg}}^{1.5}} \right)^2 \right)^{0.5} \tag{A.9}$$

The errors for the mean gas mass flow and the mean gas density along the column were determined using the standard deviation according to Equation (A.10) and (A.11) based on the geometric mean of the corresponding parameter.

$$\Delta \dot{m}_{\text{G,avg}} = \left(0.5 \cdot \left(\left(\dot{m}_{\text{G}}^{\text{T}} - \dot{m}_{\text{G,avg}} \right)^2 + \left(\dot{m}_{G}^{B} - \dot{m}_{\text{G,avg}} \right)^2 \right) \right)^{0.5} \tag{A.10}$$

$$\Delta \rho_{\text{G,avg}} = \left(0.5 \cdot \left(\left(\rho_{\text{G}}^{\text{T}} - \rho_{\text{G,avg}} \right)^2 + \left(\rho_{G}^{B} - \rho_{\text{G,avg}} \right)^2 \right) \right)^{0.5} \tag{A.11}$$

The error of the average *HETP* values was calculated according to Equation (A.12) on the basis of Equation (2.11) and (2.8).

$$\Delta HETP_{\text{avg}} = \left(\left(\frac{H_{\text{P}} \cdot \Delta\alpha_{\text{avg}}}{\alpha_{\text{avg}} \cdot \ln\left(\left(\frac{x_{\text{cHex}}^{\text{T}}}{1 - x_{\text{cHex}}^{\text{T}}} \right) \cdot \left(\frac{1 - x_{\text{cHex}}^{\text{B}}}{x_{\text{cHex}}^{\text{B}}} \right) \right)} \right)^2 + \left(\frac{H_{\text{P}} \cdot \ln\left(\alpha_{\text{avg}}\right) \cdot 2\% \cdot x_{\text{cHex}}^{\text{T}}}{\left(x_{\text{cHex}}^{\text{T}} - 1\right) \cdot x_{\text{cHex}}^{\text{T}} \cdot \ln\left(\left(\frac{x_{\text{cHex}}^{\text{T}}}{1 - x_{\text{cHex}}^{\text{T}}} \right) \cdot \left(\frac{1 - x_{\text{cHex}}^{\text{B}}}{x_{\text{cHex}}^{\text{B}}} \right) \right)^2} \right)^2 + \left(- \frac{H_{\text{P}} \cdot \ln\left(\alpha_{\text{avg}}\right) \cdot 2\% \cdot x_{\text{cHex}}^{B}}{\left(x_{\text{cHex}}^{B} - 1\right) \cdot x_{\text{cHex}}^{B} \cdot \ln\left(\left(\frac{x_{\text{cHex}}^{\text{T}}}{1 - x_{\text{cHex}}^{\text{T}}} \right) \cdot \left(\frac{1 - x_{\text{cHex}}^{\text{B}}}{x_{\text{cHex}}^{\text{B}}} \right) \right)^2} \right)^2 \right)^{0.5} \quad \text{(A.12)}$$